Baryon Number Correlation Signals in Heavy Ion Collisions

Apoorva Patel

Centre for High Energy Physics and

Supercomputer Education and Research Centre

Indian Institute of Science, Bangalore

Lattice 2012, 29 June 2012, Cairns

Reference: Phys. Rev. D 85 (2012) 114019, arXiv:1111.0177

Abstract

The flux tube model offers a pictorial description of what happens during the deconfinement phase transition in QCD. The three-point vertices of a flux tube network lead to formation of baryons upon hadronisation. Therefore, correlations in the baryon number distribution at the last scattering surface are related to the preceding pattern of the flux tube vertices, and provide a signature of the nearby deconfinement phase transition. The distribution of vertices has a simple topological feature, which suggests a two-point baryon number correlation signal that should be observable in heavy ion collisions at RHIC and LHC. Numerical simulations provide an estimate of the size of the signal.

Heavy Ion Collisions

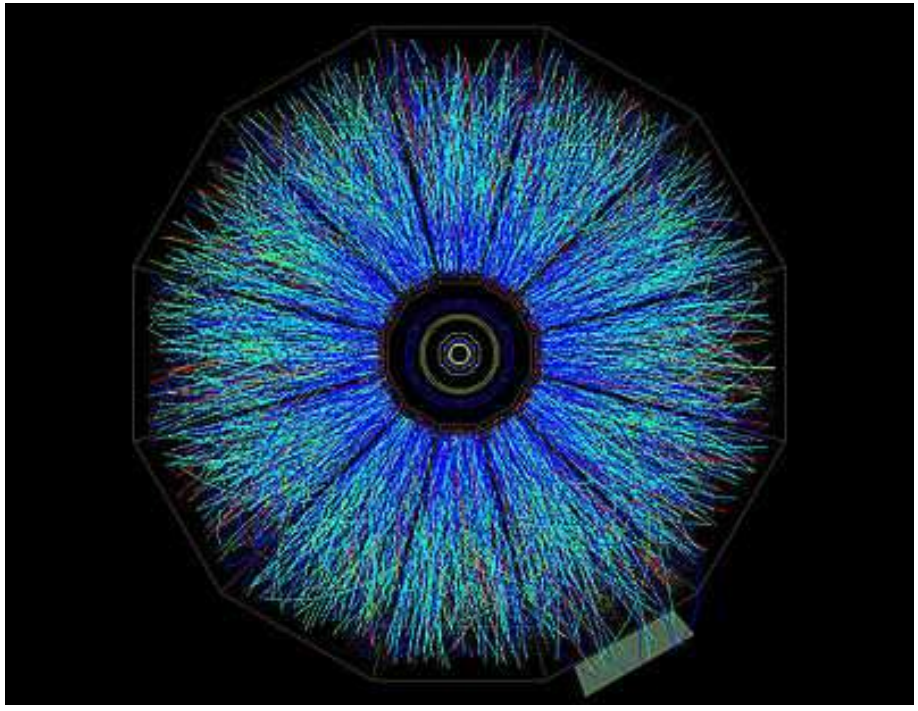

STAR event at RHIC

Au+Au collision at 100+100 GeV/nucleon

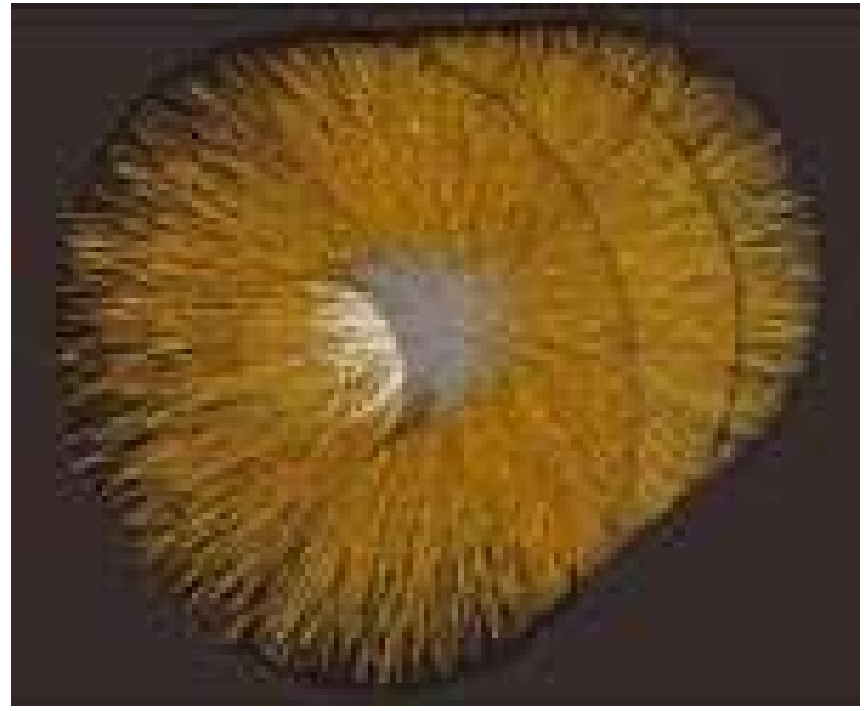

ALICE event at LHC

Pb+Pb collision at 1.38+1.38 TeV/nucleon

Thousands of hadrons are produced.
Only charged ones are detected.
Transverse coverage: $\theta_m < \theta < \pi - \theta_m$

CMBR Observations

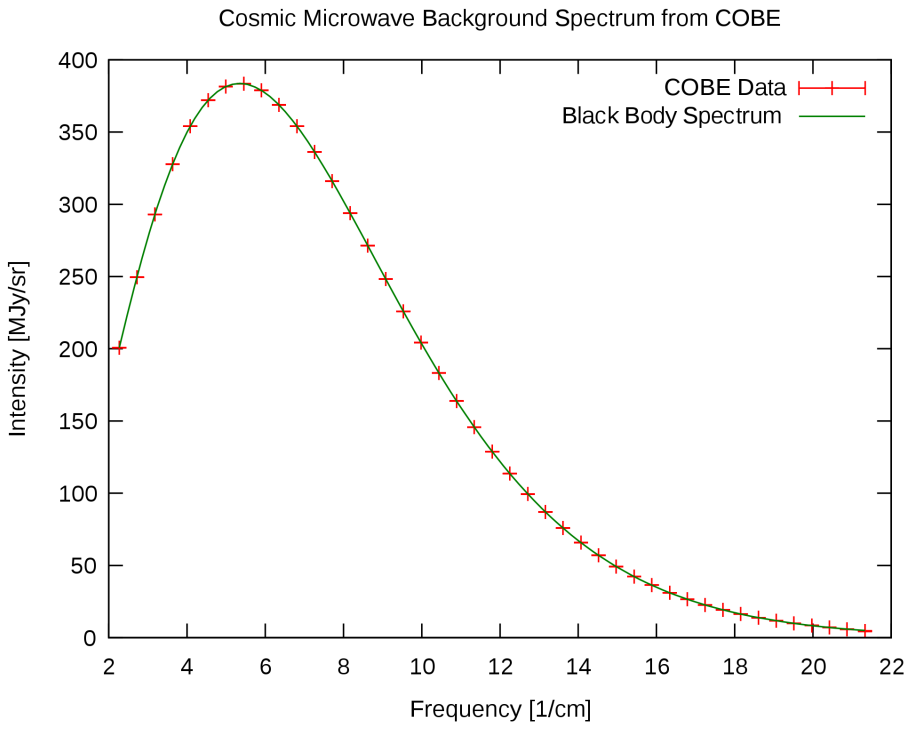

The most precisely measured black body spectrum in nature

$T = 2.72548(57)\ ^\circ K$

CMBR Observations

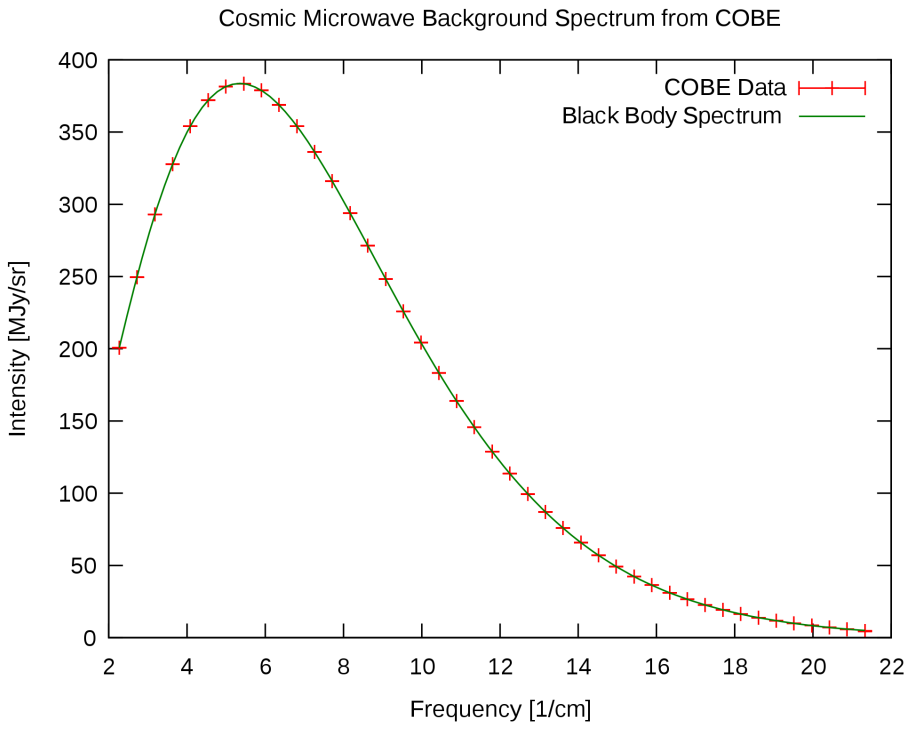

The most precisely measured black body spectrum in nature

$T = 2.72548(57)\ ^{\circ}K$

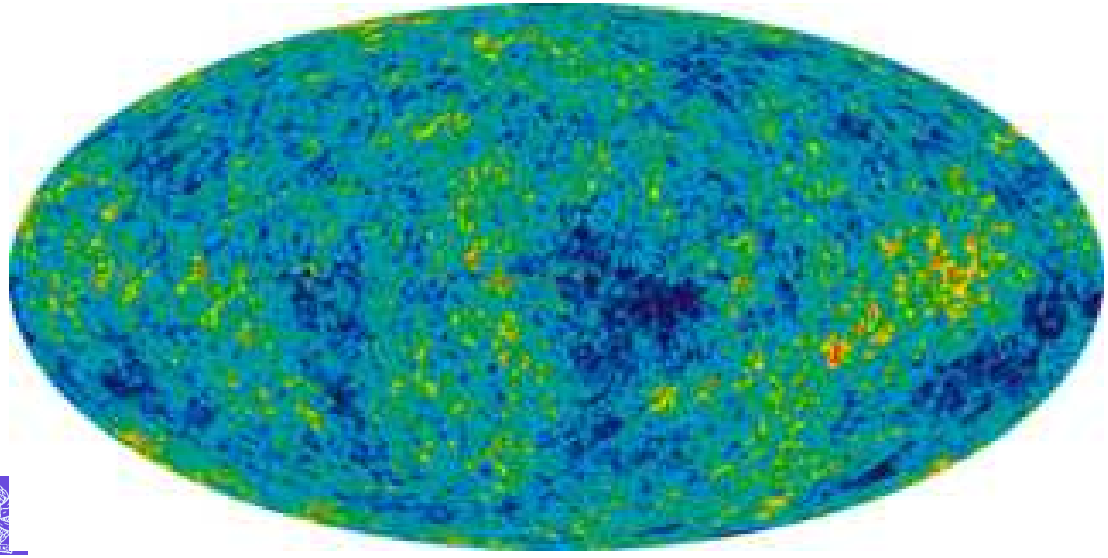

WMAP(2010) temperature anisotropy data

$\Delta T \simeq 10^{-5} T$

CMBR Angular Correlations

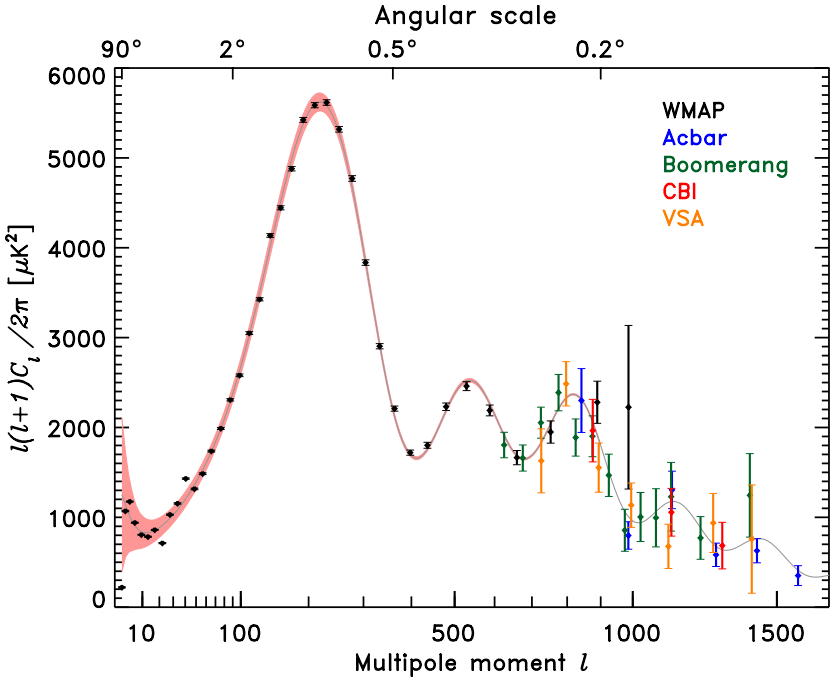

Temperature correlations (scalar) arise from the density fluctuations at the last scattering surface.

The data are accurate, and fit well to predictions of inflationary models.

CMBR Angular Correlations

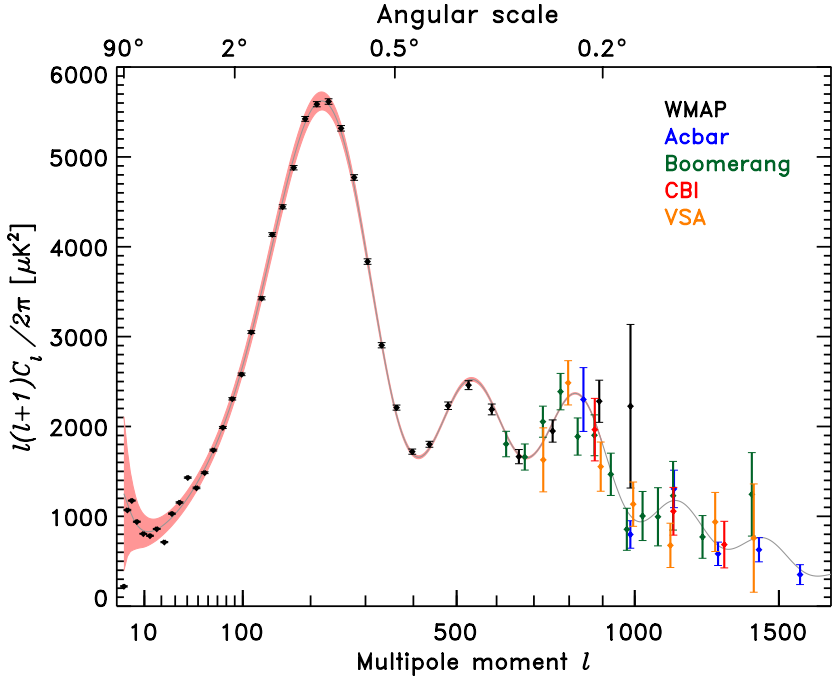

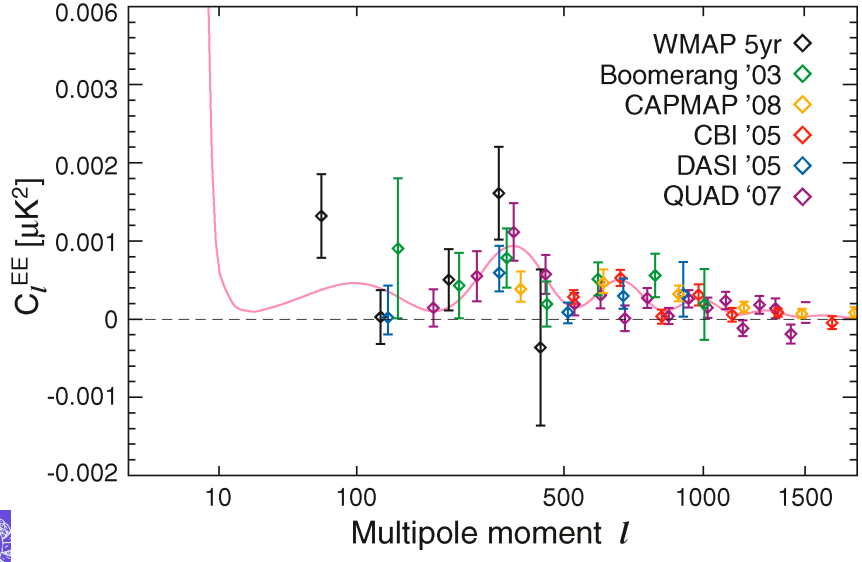

Temperature correlations (scalar) arise from the density fluctuations at the last scattering surface.

The data are accurate, and fit well to predictions of inflationary models.

Polarisation correlations (tensor) arise from scattering in the plasma at the last scattering surface.

The data are poor.

Fireball Evolution Stages

(1) Collisions are dominated by low$-x$ high density gluons. Coherent saturated gluons form Colour Glass Condensate.

$\tau < 0.1$ fm/c

Fireball Evolution Stages

(1) Collisions are dominated by low$-x$ high density gluons. Coherent saturated gluons form Colour Glass Condensate.

$\tau < 0.1$ fm/c

(2) Strong longitudinal colour electric and colour magnetic fields relax. Non-zero impact parameter produces elliptic flow in the overlap region. Topological excitations and energy density fluctuations in the Glasma thermalise by hydrodynamic evolution.

$\tau = 0.1 - 1$ fm/c

Fireball Evolution Stages

(1) Collisions are dominated by low$-x$ high density gluons. Coherent saturated gluons form Colour Glass Condensate.

$\tau < 0.1$ fm/c

(2) Strong longitudinal colour electric and colour magnetic fields relax. Non-zero impact parameter produces elliptic flow in the overlap region. Topological excitations and energy density fluctuations in the Glasma thermalise by hydrodynamic evolution.

$\tau = 0.1 - 1$ fm/c

(3) Quasi-equilibrium quark-gluon plasma has energy density $\epsilon \simeq 1\mathrm{GeV}/\mathrm{fm}^3$ and $T_{\mathrm{cr}} \simeq 175\mathrm{MeV}$.

$\tau = 1 - 10$ fm/c

Fireball Evolution Stages

(1) Collisions are dominated by low$-x$ high density gluons. Coherent saturated gluons form Colour Glass Condensate.

$\tau < 0.1$ fm/c

(2) Strong longitudinal colour electric and colour magnetic fields relax. Non-zero impact parameter produces elliptic flow in the overlap region. Topological excitations and energy density fluctuations in the Glasma thermalise by hydrodynamic evolution.

$\tau = 0.1 - 1$ fm/c

(3) Quasi-equilibrium quark-gluon plasma has energy density $\epsilon \simeq 1\mathrm{GeV}/\mathrm{fm}^3$ and $T_{\mathrm{cr}} \simeq 175\mathrm{MeV}$.

$\tau = 1 - 10$ fm/c

(4) Hadronisation reduces entropy density and expands the fireball. Inelastic scattering stops, and species abundances get fixed, by chemical freeze-out at $T_{\mathrm{chem}} \simeq 170\mathrm{MeV}$.

$\tau > 10$ fm/c

Fireball Evolution Stages

(1) Collisions are dominated by low$-x$ high density gluons. Coherent saturated gluons form Colour Glass Condensate.

$\tau < 0.1$ fm/c

(2) Strong longitudinal colour electric and colour magnetic fields relax. Non-zero impact parameter produces elliptic flow in the overlap region. Topological excitations and energy density fluctuations in the Glasma thermalise by hydrodynamic evolution.

$\tau = 0.1 - 1$ fm/c

(3) Quasi-equilibrium quark-gluon plasma has energy density $\epsilon \simeq 1\mathrm{GeV}/\mathrm{fm}^3$ and $T_{\mathrm{cr}} \simeq 175\mathrm{MeV}$.

$\tau = 1 - 10$ fm/c

(4) Hadronisation reduces entropy density and expands the fireball. Inelastic scattering stops, and species abundances get fixed, by chemical freeze-out at $T_{\mathrm{chem}} \simeq 170\mathrm{MeV}$.

$\tau > 10$ fm/c

(5) Elastic and resonant scattering (mediated largely by pions) ceases, with kinetic freeze-out at $T_{\mathrm{kin}} \simeq 120\mathrm{MeV}$.

Experimental Signals

Multiplicities and distributions of various particles are detected. Only charged hadrons observed in sufficiently transverse directions (to avoid the unscattered beams).

Photons and leptons are also observed through their electromagnetic interactions.

Glauber model used to infer the centrality of the collisions (no. of participants) from the charged particle multiplicities.

Experimental Signals

Multiplicities and distributions of various particles are detected. Only charged hadrons observed in sufficiently transverse directions (to avoid the unscattered beams).

Photons and leptons are also observed through their electromagnetic interactions.

Glauber model used to infer the centrality of the collisions (no. of participants) from the charged particle multiplicities.

(a) Initial approach to equilibrium signals: Direct photons and leptons, heavy quark jets, high p_T jets, the elliptic flow.
(b) Quasi-equilibrated QGP signals: Moderate p_T hadrons produced close to the fireball surface.

Experimental Signals

Multiplicities and distributions of various particles are detected. Only charged hadrons observed in sufficiently transverse directions (to avoid the unscattered beams).

Photons and leptons are also observed through their electromagnetic interactions.

Glauber model used to infer the centrality of the collisions (no. of participants) from the charged particle multiplicities.

(a) Initial approach to equilibrium signals: Direct photons and leptons, heavy quark jets, high p_T jets, the elliptic flow.
(b) Quasi-equilibrated QGP signals: Moderate p_T hadrons produced close to the fireball surface.

Temperature information is extracted from particle abundances ($T_{\rm chem}$) and energy-momentum distributions ($T_{\rm kin}$), using thermalised hadron resonance gas models.

Angular distributions can see through the scatterings to the correlation patterns in the QGP (assuming low diffusion).

Types of observables

Specific patterns in the distribution of hadrons can be searched for, using techniques similar to those used to analyse the temperature fluctuations in the CMBR.

Types of observables

Specific patterns in the distribution of hadrons can be searched for, using techniques similar to those used to analyse the temperature fluctuations in the CMBR.

One-point observables:

Particle multiplicities (enhancements, suppressions)
Particle number fluctuations (susceptibilities)
Distributions of conserved charges ($n_u, n_d, n_s \leftrightarrow Q, B, S$)
Energy-momentum distributions and jets
Angular distributions (elliptic flow and harmonics)

Types of observables

Specific patterns in the distribution of hadrons can be searched for, using techniques similar to those used to analyse the temperature fluctuations in the CMBR.

One-point observables:

Particle multiplicities (enhancements, suppressions)
Particle number fluctuations (susceptibilities)
Distributions of conserved charges ($n_u, n_d, n_s \leftrightarrow Q, B, S$)
Energy-momentum distributions and jets
Angular distributions (elliptic flow and harmonics)

Two-point observables:

Angular correlations for particles and charges
(e.g. ridge, jet quenching, Hanbury-Brown–Twiss effect)

Sum rules relate two-point observables to one-point ones (e.g. correlations to susceptibilities).

QCD Phase Structure

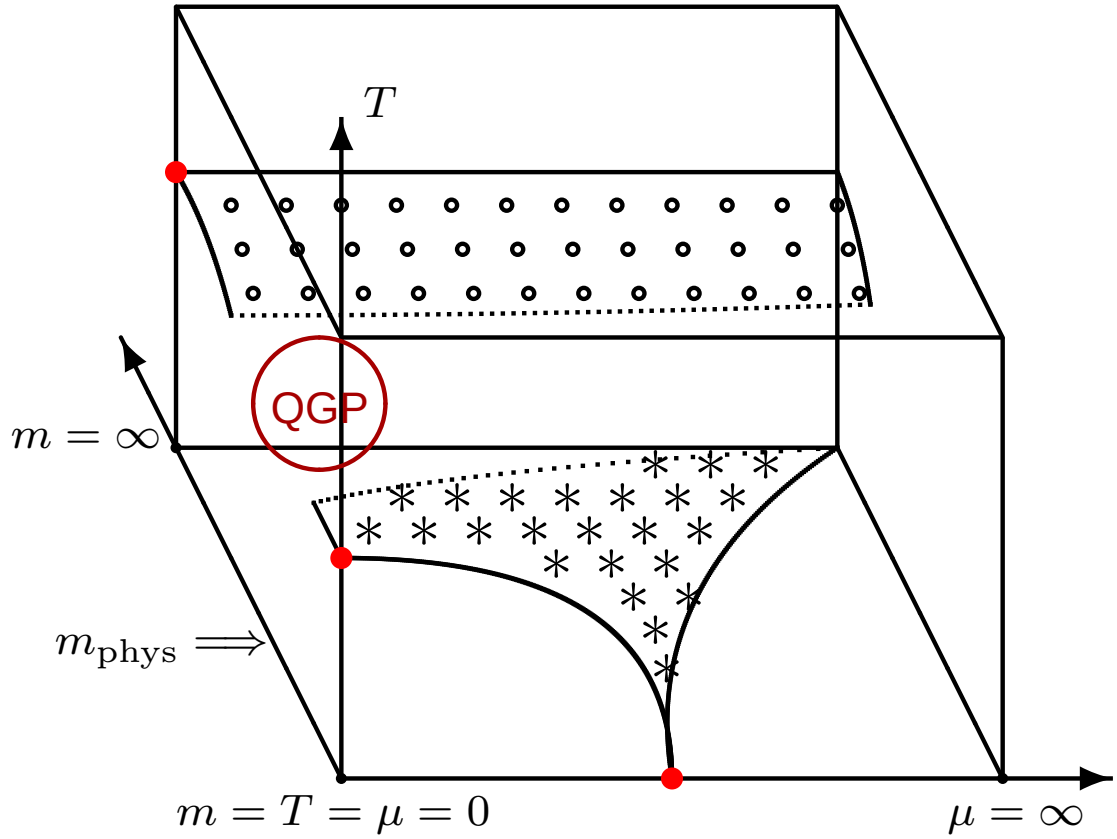

Schematic description of the phase structure of QCD in the $m - T - \mu$ space.
First order transition surfaces are shown shaded, and critical lines are shown dotted.
Colour superconductor phases occurring at large chemical potential are omitted.
RHIC and LHC experiments belong to the cross-over region.

QCD Phase Transitions

(1) $m = \infty$, $N \geq 3$: First order finite temperature deconfinement transition, governed by the breaking of the global Z_N centre symmetry of the Polyakov loop.

(2) $m = 0 = \mu$, $N_f \geq 3$: First order finite temperature chiral transition, governed by the restoration of the flavour $SU(N_f)_V$ symmetry to $SU(N_f)_L \otimes SU(N_f)_R$.

(3) $m = 0 = T$, $\mu \simeq$ constituent quark mass: First order baryon condensation phase transition, where the vacuum structure changes from $\langle \bar{\psi}\psi \rangle \neq 0$ to $\langle \psi^\dagger \psi \rangle \neq 0$.

First order phase transitions are stable against small changes of symmetry breaking perturbations. The above three transitions extend inward, to varying extent, from the boundaries of the phase structure.

No phase transition for the physical values of the quark masses (unless μ is sufficiently large). But the three nearby transitions have their imprints in the cross-over region.

Flux Tubes in QCD

QCD exhibits dual superconductivity with linearly confined colour-electric flux. (Nambu, 't Hooft, Mandelstam)

Lattice QCD calculations show area law for Wilson loops, analytically at strong coupling and numerically at weak coupling. The characteristic scale is $r \geq 0.5$fm.

Flux Tubes in QCD

QCD exhibits dual superconductivity with linearly confined colour-electric flux. (Nambu, 't Hooft, Mandelstam)

Lattice QCD calculations show area law for Wilson loops, analytically at strong coupling and numerically at weak coupling. The characteristic scale is $r \geq 0.5$fm.

Meson and baryon wavefunctions are represented by the invariant tensors δ_{ab} and ϵ_{abc}. Other multi-quark hadrons (except for nuclei) are phenomenologically not prominent.

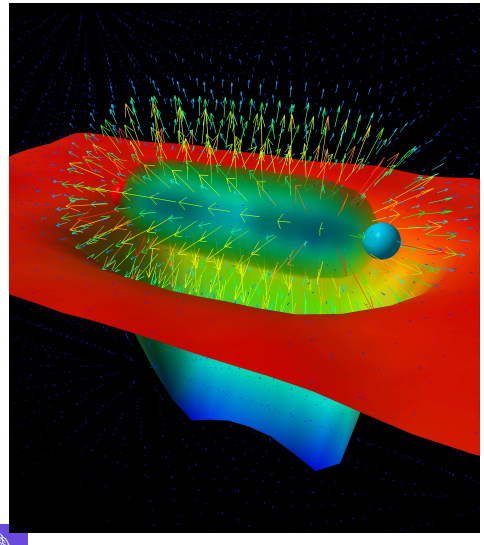

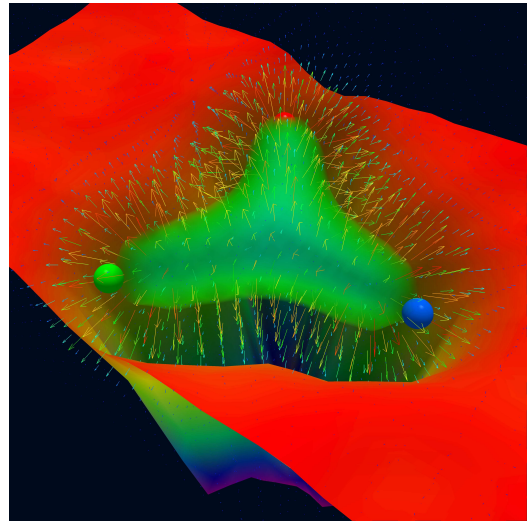

F. Bissey, F.G. Cao, A.R. Kitson, A.I Signal, D.B. Leinweber, B.G. Lassock and A.G. Williams, Phys. Rev. D 76 (2007) 114512.

Flux Tube Configurations

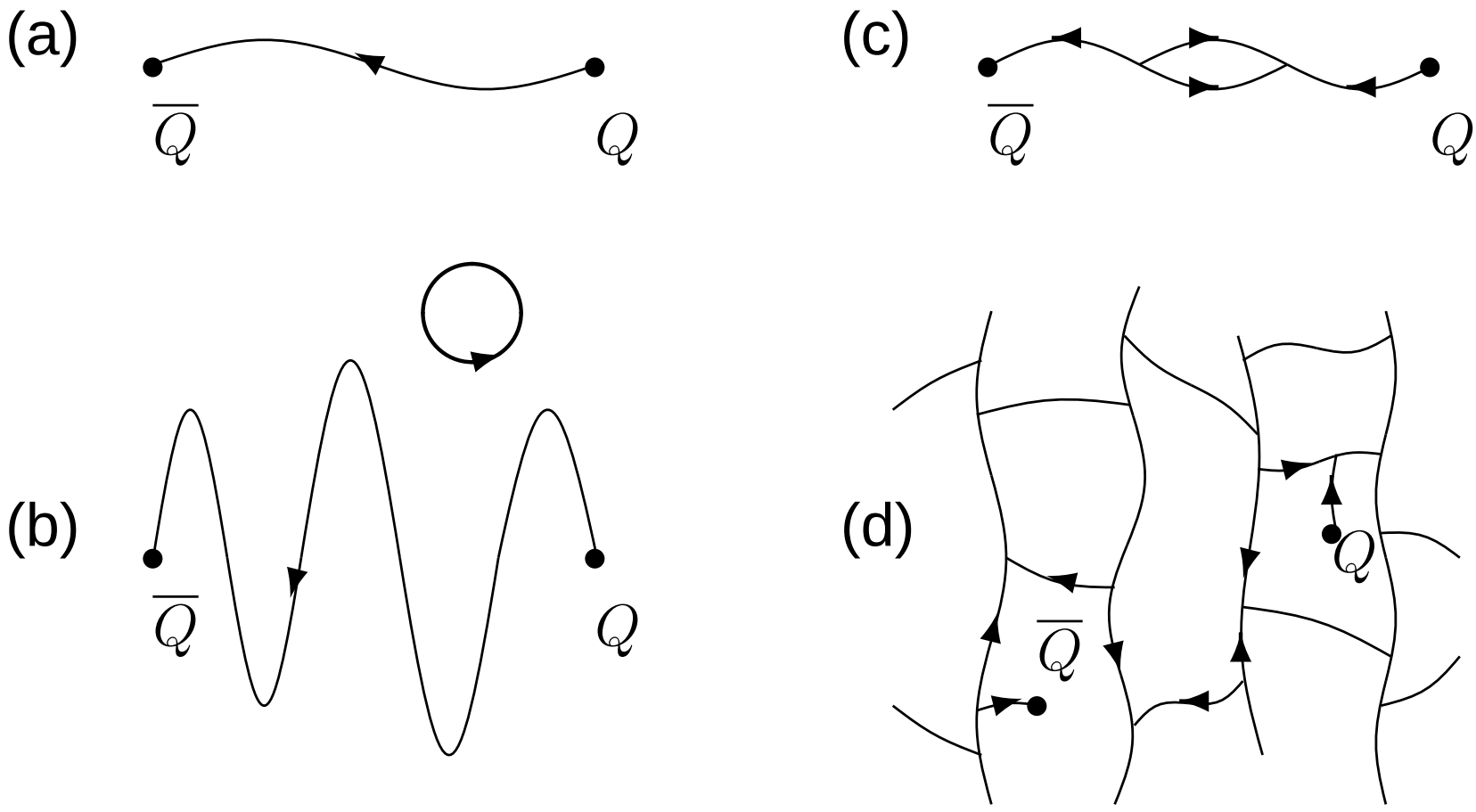

Possible flux tube configurations connecting a static quark-antiquark pair, as the temperature is increased (from top to bottom), and when baryonic vertices are included (from left to right).

Flux Tube Breaking

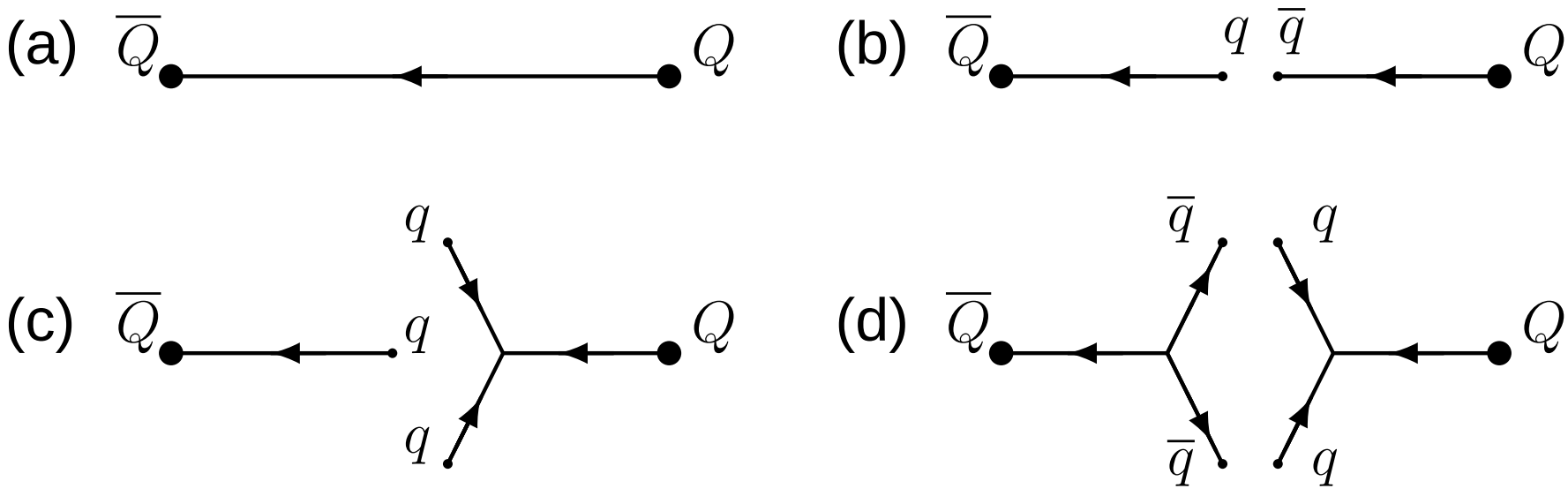

A colour-electric flux tube can break when dynamical quarks are included in QCD.

(a) A flux tube produced by static colour sources.

(b) Its breaking by a quark-antiquark pair appearing from the vacuum.

(c) Its breaking by a baryon appearing from the vacuum at finite chemical potential.

(d) Breaking of a vertex-antivertex flux tube bubble by two quark-antiquark pairs.

[In reality, baryon number is conserved, and baryon-antibaryon pairs are produced. Hadronization models incorporate that using effective diquark degrees of freedom.]

Deconfinement Phase Transition

Finite temperature behaviour of QCD is governed by the competition between energy and entropy of the flux tube configurations.

With increasing temperature, the flux tubes oscillate more and also produce more vertices.

Deconfinement means a quark-antiquark pair loses information about each-other's position.

Deconfinement Phase Transition

Finite temperature behaviour of QCD is governed by the competition between energy and entropy of the flux tube configurations.

With increasing temperature, the flux tubes oscillate more and also produce more vertices.

Deconfinement means a quark-antiquark pair loses information about each-other's position.

Second order phase transition corresponds to flux tubes of diverging length. First order phase transition corresponds to a percolating flux tube network.

Deconfinement Phase Transition

Finite temperature behaviour of QCD is governed by the competition between energy and entropy of the flux tube configurations.
With increasing temperature, the flux tubes oscillate more and also produce more vertices.
Deconfinement means a quark-antiquark pair loses information about each-other's position.

Second order phase transition corresponds to flux tubes of diverging length. First order phase transition corresponds to a percolating flux tube network.

Light dynamical quarks break up long flux tubes, changing the deconfinement phase transition into a cross-over.
Still large enough clusters of flux tubes may arise at $m_{\rm phys}$, as a consequence of the nearby phase transition.

Flux Tube Model Variables

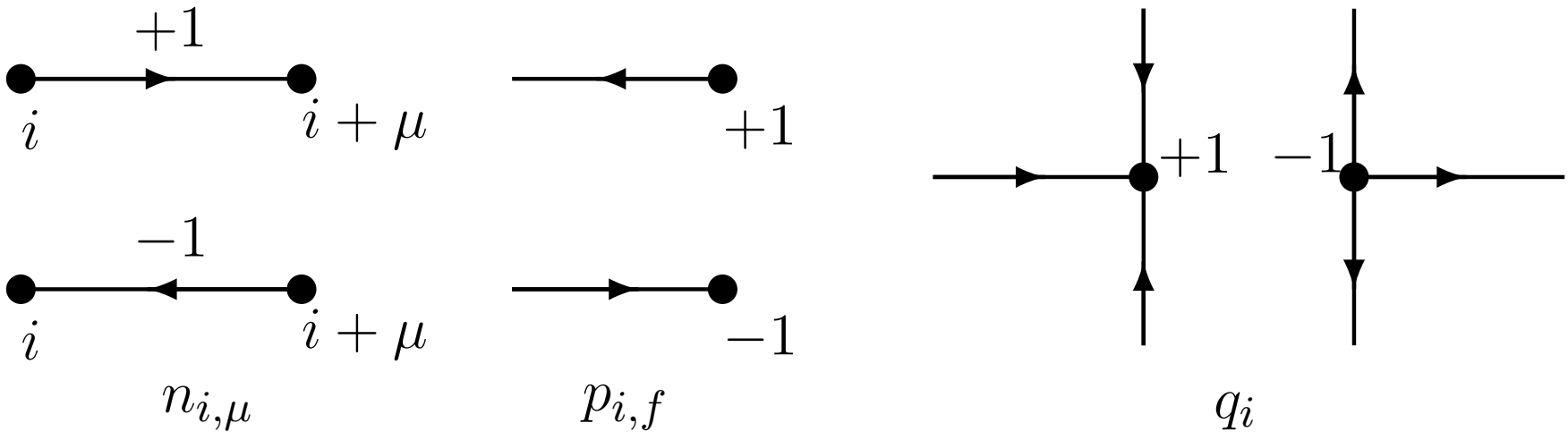

The link and site variables for the flux tube model.

Energy: $E = \sigma a \sum_{i,\mu} |n_{i,\mu}| + m \sum_{i,f} |p_{i,f}| + v \sum_i |q_i|$

Gauss's Law: $\sum_\mu (n_{i,\mu} - n_{i-\mu,\mu}) - \sum_f p_{i,f} + N q_i \equiv \alpha_i = 0$

Baryon Number: $B = \frac{1}{N} \sum_{i,f} p_{i,f} = \sum_i q_i$

Grand Canonical Partition Function

$$Z[T,\mu] = \sum_{n_{i,\mu},\ p_{i,f},\ q_i} \exp\left[-\frac{1}{T}(E-\mu NB)\right] \prod_i \delta_{\alpha_i,0}$$

The constraint can be solved by changing to dual variables:

$$\delta_{\alpha_i,0} = \int_{-\pi}^{\pi} \frac{d\theta_i}{2\pi}\ e^{i\alpha_i\theta_i}$$

Sum over $n_{i,\mu},\ p_{i,f},\ q_i$ can then be explicitly carried out:

$$Z[T,\mu] = \int_{-\pi}^{\pi} \prod_i \frac{d\theta_i}{2\pi} \prod_{i,\mu}(1+2e^{-\sigma a/T}\cos(\theta_{i+\mu}-\theta_i))\times$$

$$\times \prod_i \left(1+2e^{-m/T}\cos\left(\theta_i + i\frac{\mu}{T}\right)\right)^{2N_f} \prod_i (1+2e^{-v/T}\cos(N\theta_i))$$

Phenomenological Features

The model is in the universality class of the XY spin model, with an ordinary and a $Z(N)$ symmetric magnetic field.

$$Z[T,\mu] = \int_{-\pi}^{\pi} \prod_i \frac{d\theta_i}{2\pi} \; \exp\Big[J \sum_{i,\mu} \cos(\theta_{i+\mu} - \theta_i) + \\ + h \sum_i \cos\left(\theta_i + i\frac{\mu}{T}\right) + p \sum_i \cos(N\theta_i) \Big]$$

$$J \simeq 2e^{-\sigma a/T} \;, \quad h \simeq 4N_f \; e^{-m/T} \;, \quad p \simeq 2e^{-v/T}$$

Phenomenological Features

The model is in the universality class of the XY spin model, with an ordinary and a $Z(N)$ symmetric magnetic field.

$$Z[T,\mu] = \int_{-\pi}^{\pi} \prod_i \frac{d\theta_i}{2\pi} \; \exp\Big[J \sum_{i,\mu} \cos(\theta_{i+\mu} - \theta_i) + \\ + h \sum_i \cos\left(\theta_i + i\frac{\mu}{T}\right) + p \sum_i \cos(N\theta_i) \Big]$$

$$J \simeq 2e^{-\sigma a/T} \;, \quad h \simeq 4N_f \; e^{-m/T} \;, \quad p \simeq 2e^{-v/T}$$

Introduction of a static quark source at site j modifies the Gauss's law constraint there as $\delta_{\alpha_j,0} \to \delta_{\alpha_j,-1}$.

Its free energy is given by $\exp(-F_q/T) = \langle \exp(-i\theta_j) \rangle$.

So θ_i corresponds to the phase of the Polyakov loop.

Flux tube and Polyakov loop descriptions of deconfinement in finite temperature gauge theory are dual to each other.

Baryon Number Correlations

Focus on the position space picture of the flux tube network.

In every flux tube cluster, any neighbour of a vertex is an anti-vertex and vice versa. Production and annihilation of vertices stops at chemical freeze-out. Thereafter, every vertex yields a baryon and every anti-vertex an antibaryon.

Baryon Number Correlations

Focus on the position space picture of the flux tube network.

In every flux tube cluster, any neighbour of a vertex is an anti-vertex and vice versa. Production and annihilation of vertices stops at chemical freeze-out. Thereafter, every vertex yields a baryon and every anti-vertex an antibaryon.

In absence of large scale diffusion, radial propagation of (anti)baryons preserves the geometric pattern of (anti)vertices present at the chemical freeze-out stage.

Angular positions of (anti)baryons seen in the detector can be backtracked to the angular positions of (anti)vertices that emerge from the QGP fireball.

Baryon Number Correlations

Focus on the position space picture of the flux tube network.

In every flux tube cluster, any neighbour of a vertex is an anti-vertex and vice versa. Production and annihilation of vertices stops at chemical freeze-out. Thereafter, every vertex yields a baryon and every anti-vertex an antibaryon.

In absence of large scale diffusion, radial propagation of (anti)baryons preserves the geometric pattern of (anti)vertices present at the chemical freeze-out stage.

Angular positions of (anti)baryons seen in the detector can be backtracked to the angular positions of (anti)vertices that emerge from the QGP fireball.

Heavy ion collisions produce a sizeable number of antibaryons, from an initial state that has none, implying (a) the fireball produces a good number of (anti)vertices, (b) fragmentation of flux tubes during hadronisation is more likely than annihilation of vertex-antivertex pairs.

Pair Distribution Function

Density: $\rho(\vec{r}) = \left\langle \sum_\alpha \delta(\vec{r} - \vec{r}_i) \right\rangle$

Correlation: $\rho(\vec{r})\ g(\vec{r}, \vec{r}')\ \rho(\vec{r}') = \left\langle \sum_{i \neq j} \delta(\vec{r} - \vec{r}_i)\ \delta(\vec{r}' - \vec{r}_j) \right\rangle$

In homogeneous and isotropic fluids, ρ is independent of $\vec{r}$ and g depends only on $|\vec{r} - \vec{r}'|$, resulting in

$$\rho\ g(r) = \left\langle \sum_{i \neq 0} \delta(\vec{r} - \vec{r}_i) \right\rangle$$

Pair Distribution Function

Density: $\rho(\vec{r}) = \left\langle \sum_\alpha \delta(\vec{r} - \vec{r}_i) \right\rangle$

Correlation: $\rho(\vec{r})\ g(\vec{r}, \vec{r}')\ \rho(\vec{r}') = \left\langle \sum_{i \neq j} \delta(\vec{r} - \vec{r}_i)\ \delta(\vec{r}' - \vec{r}_j) \right\rangle$

In homogeneous and isotropic fluids, ρ is independent of $\vec{r}$ and g depends only on $|\vec{r} - \vec{r}'|$, resulting in

$$\rho\ g(r) = \left\langle \sum_{i \neq 0} \delta(\vec{r} - \vec{r}_i) \right\rangle$$

Asymptotically, $g(r \to \infty) = 1$ (interactions fade away).

For an ideal gas with no correlations, $g(r) = 1$.

For objects with hard-core repulsion, $g(0) = 0$, and beyond the hard core $g(r)$ tends to its asymptotic value 1, exhibiting damped oscillations.

Pair Distribution Function

Density: $\rho(\vec{r}) = \left\langle \sum_\alpha \delta(\vec{r} - \vec{r}_i) \right\rangle$

Correlation: $\rho(\vec{r})\ g(\vec{r}, \vec{r}')\ \rho(\vec{r}') = \left\langle \sum_{i \neq j} \delta(\vec{r} - \vec{r}_i)\ \delta(\vec{r}' - \vec{r}_j) \right\rangle$

In homogeneous and isotropic fluids, ρ is independent of $\vec{r}$ and g depends only on $|\vec{r} - \vec{r}'|$, resulting in

$$\rho\ g(r) = \left\langle \sum_{i \neq 0} \delta(\vec{r} - \vec{r}_i) \right\rangle$$

Asymptotically, $g(r \to \infty) = 1$ (interactions fade away).
For an ideal gas with no correlations, $g(r) = 1$.
For objects with hard-core repulsion, $g(0) = 0$, and beyond the hard core $g(r)$ tends to its asymptotic value 1, exhibiting damped oscillations.

For baryon number distributions, $g_{|v|}$ is a correlation insensitive reference function, while g_v (vertex signs $q_i q_j$ included) is sensitive to vertex-antivertex correlations.
The contrast between the two measures the correlations.

Theoretical Expectations

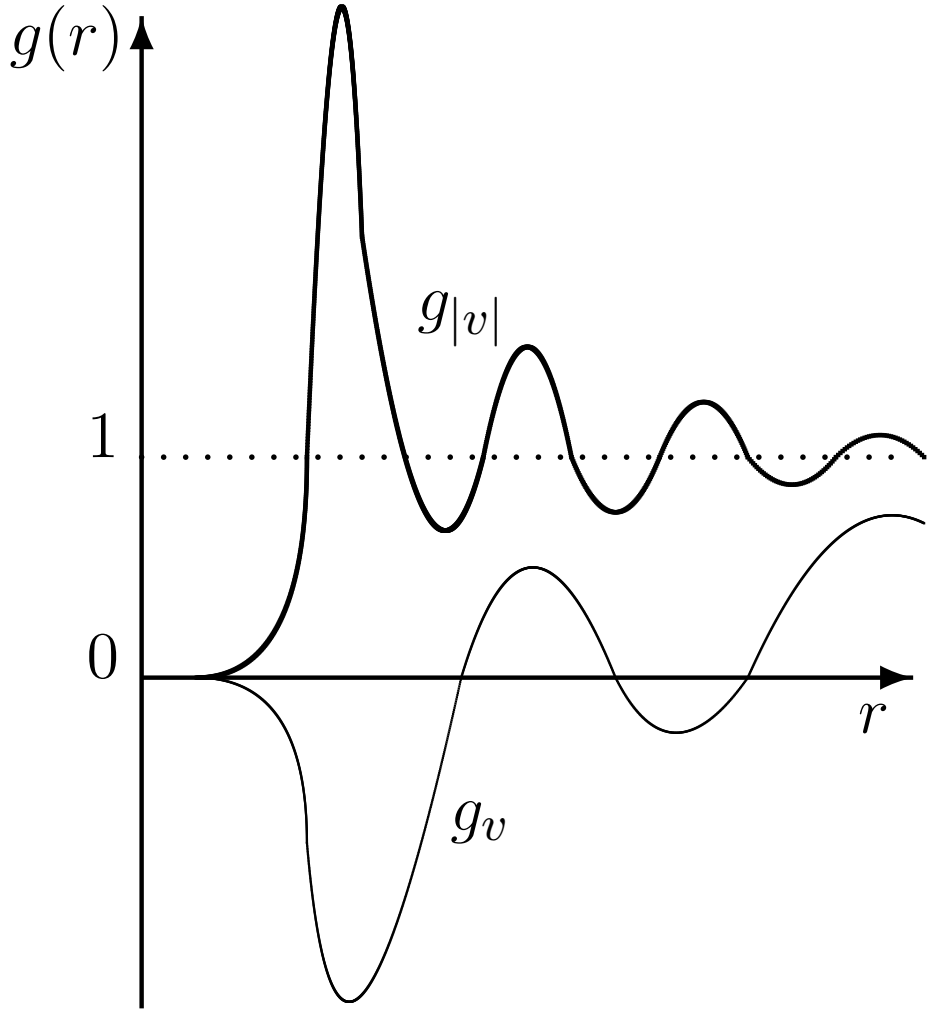

Positions of peaks quantify separations of neighbours.

Widths of peaks measure hard/soft nature of objects.

The first peak is the most informative.

Schematic representation of the pair distribution functions $g_{|v|}(r)$ and $g_v(r)$. The former is similar to that for objects with hard-core repulsion. The latter is for a percolating flux tube network where vertices and anti-vertices alternate (similar to charges in ionic liquids).

Angular Projection

Projection of 3-dimensional pair distribution function onto the surface of the fireball smears its oscillatory structure.

$$w(\alpha) = \int_{r_{\min}}^{r_{\max}} S(\alpha, r)\; g(r)\; dr\;, \quad \int_0^{\pi} S(\alpha, r)\; d\alpha = 1$$

$$\cos\alpha = \cos\theta\cos\theta' + \sin\theta\sin\theta'\cos(\phi - \phi')$$

Angular Projection

Projection of 3-dimensional pair distribution function onto the surface of the fireball smears its oscillatory structure.

$$w(\alpha) = \int_{r_{\rm min}}^{r_{\rm max}} S(\alpha, r)\; g(r)\; dr\;, \quad \int_0^{\pi} S(\alpha, r)\; d\alpha = 1$$

$$\cos\alpha = \cos\theta\cos\theta' + \sin\theta\sin\theta'\cos(\phi - \phi')$$

When inter-vertex separation $r \ll$ the fireball radius R,

$$S(\alpha, r) = \int_0^R \frac{3a^2 da}{R^3} \int_0^{\pi} \frac{\sin\beta\; d\beta}{2}\; \delta\left(\alpha - \frac{r}{a}\sin\beta\right)$$

$$= \begin{cases} 9\pi r^3/(16R^3\alpha^4) & : \alpha \geq r/R \\ 3r^3\left(12\lambda - 8\sin(2\lambda) + \sin(4\lambda)\right)/(32R^3\alpha^4) & : \sin\lambda = \alpha R/r \leq 1 \end{cases}$$

Internucleon separation in nuclear matter is ~ 2fm.
Fireball radius in central heavy ion collisions is ~ 6fm.

Data Parametrisation

The experimental set up has axial symmetry around the beam axis, and reflection (parity) symmetry $\theta \leftrightarrow \pi - \theta$.

$$b(\hat{n}) \equiv b(\theta, \phi) = \frac{1}{\sqrt{2\pi}} \sum_{\sigma=\pm} \sum_{m=-\infty}^{\infty} b_m^{\sigma}(\theta)\, e^{im\phi} \;,\; \langle b(\hat{n}) \rangle = \frac{b_0^{+}(\theta)}{\sqrt{2\pi}}$$

Data Parametrisation

The experimental set up has axial symmetry around the beam axis, and reflection (parity) symmetry $\theta \leftrightarrow \pi - \theta$.

$$b(\hat{n}) \equiv b(\theta, \phi) = \frac{1}{\sqrt{2\pi}} \sum_{\sigma=\pm} \sum_{m=-\infty}^{\infty} b_m^\sigma(\theta)\, e^{im\phi}\ ,\ \langle b(\hat{n}) \rangle = \frac{b_0^+(\theta)}{\sqrt{2\pi}}$$

Two-point correlations:

$$\langle b(\hat{n}) b(\hat{n}') \rangle = \frac{1}{2\pi} \sum_{\sigma=\pm} \sum_{m=-\infty}^{\infty} C_m^\sigma(\theta, \theta')\, e^{im(\phi-\phi')}$$

$$C_m^\sigma(\theta, \theta') = \frac{1}{2\pi} \int_0^{2\pi} d\phi \int_0^{2\phi} d\phi'\ e^{-im(\phi-\phi')} \langle b^\sigma(\hat{n}) b^\sigma(\hat{n}') \rangle$$

$$[C_m^\sigma(\theta, \theta')]_c = C_m^\sigma(\theta, \theta')\ -\ \delta_{m0}\, \delta_{\sigma+}\, b_0^+(\theta)\, b_0^+(\theta')$$

$C_m^\sigma(\theta, \theta')$ can be expanded in terms of Associated Legendre polynomials for homogeneous isotropic distributions.

Gaps Between Theory and Experiment

Major hurdle:

Detectors observe protons and anti-protons, but not neutrons and anti-neutrons. Baryon number correlations can be extracted only if the observed subset is a faithful representation (ideally proportional) of the total distribution.

Gaps Between Theory and Experiment

Major hurdle:
Detectors observe protons and anti-protons, but not neutrons and anti-neutrons. Baryon number correlations can be extracted only if the observed subset is a faithful representation (ideally proportional) of the total distribution.

There are other practical corrections.
Correlations are weakened by:
(1) Only approximate equilibration of the fireball,
(2) Non-uniformity of the QGP due to the elliptic flow,
(3) Baryon number diffusion after hadronisation,
and strengthened by:
(4) Development of hard baryon core during hadronisation.

Gaps Between Theory and Experiment

Major hurdle:
Detectors observe protons and anti-protons, but not neutrons and anti-neutrons. Baryon number correlations can be extracted only if the observed subset is a faithful representation (ideally proportional) of the total distribution.

There are other practical corrections.
Correlations are weakened by:
(1) Only approximate equilibration of the fireball,
(2) Non-uniformity of the QGP due to the elliptic flow,
(3) Baryon number diffusion after hadronisation,
and strengthened by:
(4) Development of hard baryon core during hadronisation.

Low diffusion and low viscosity are compatible because of high entropy of hadronic medium.
Einstein-Stokes relation: $D = kT/(6\pi\eta r)$. For the RHIC and LHC data:

$\eta/s \lesssim 0.4\hbar/k$, $\eta = 5 \times 10^{11}$Pa.s, $r = 1$fm, $T = 170$MeV $\Rightarrow D = 10^{-2}$c.fm

Despite these gaps . . .

(a) There is no fundamental interaction associated with the baryon number. So the correlations have to arise from the preceding dynamics of QCD in the QGP phase.
(b) The vertex-antivertex correlation is a topological feature, robust against many details of the dynamics.

Despite these gaps . . .

(a) There is no fundamental interaction associated with the baryon number. So the correlations have to arise from the preceding dynamics of QCD in the QGP phase.
(b) The vertex-antivertex correlation is a topological feature, robust against many details of the dynamics.

Correlation signal parameters:
(1) Peak position (interbaryon separation): $\simeq 2$fm.
(2) Peak height (tightness of packing): Estimate needed.

Despite these gaps . . .

(a) There is no fundamental interaction associated with the baryon number. So the correlations have to arise from the preceding dynamics of QCD in the QGP phase.
(b) The vertex-antivertex correlation is a topological feature, robust against many details of the dynamics.

Correlation signal parameters:
(1) Peak position (interbaryon separation): $\simeq 2$fm.
(2) Peak height (tightness of packing): Estimate needed.

It is worthwhile to look for the two-point baryon number correlations in the experimental data, as a characteristic signature of the deconfinement phase transition, without worrying about accurate prediction of its magnitude.

Bipartite graph:

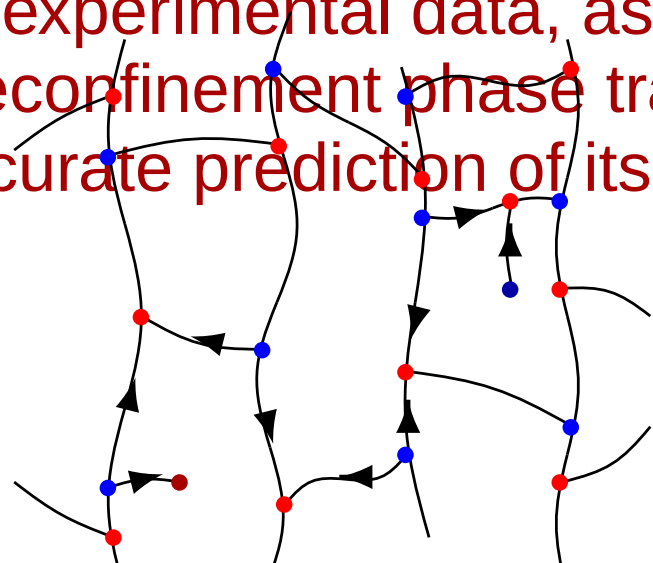

References

QCD Phase Structure:

M. Alford, A. Schmitt, K. Rajagopal and T. Schäfer, Rev. Mod. Phys. 80 (2008) 1455.

D. Kharzeev, Proc. *The 18th Particles and Nuclei International Conference, PANIC08*, Eilat, Nucl. Phys. A 827 (2009) 118c.

L. McLerran, Proc. *The Sixth International Conference on the Physics and Astrophysics of Quark Gluon Plasma*, Goa, Nucl. Phys. A 862-863 (2011) 251.

C. Loizides, Proc. *23rd Rencontres de Blois, Particle Physics and Cosmology*, Blois, (2011).

S. Gupta, Proc. *The XXVIIIth International Symposium on Lattice Field Theory*, Villasimius, PoS (Lattice 2010) 007.

K. Kanaya, Proc. *The XXVIII International Symposium on Lattice Field Theory*, Villasimius, PoS (Lattice 2010) 012.

Flux Tube Description:

G. Ripka, *Dual Superconductor Models of Color Confinement*, Lecture Notes in Physics, Vol. 639, (Springer, Berlin, 2004).

A. Patel, Nucl. Phys. B 243 (1984) 411.

A. Patel, Phys. Lett. 139B (1984) 394.

A. Patel, Proc. *International Conference on the Physics and Astrophysics of Quark-Gluon Plasma*, Bombay, (World Scientific, Singapore, 1988), p.135.

Lattice QCD Based Models:

J. Condella and C. DeTar, Phys. Rev. D 61 (2000) 074023.

M. Alford, S. Chandrasekharan, J. Cox and U.-J. Wiese, Nucl. Phys. B 602 (2001) 61.

S. Kim, P. de Forcrand, S. Kratochvila and T. Takaishi, Proc. *The XXIIIrd International Symposium on Lattice Field Theory*, Dublin, PoS (Lattice 2005) 166.

Y.D. Mercado, H.G. Evertz and C. Gattringer, Phys. Rev. Lett. 106 (2011) 222001.

P.N. Meisinger and M.C. Ogilvie, Phys. Lett. B 379 (2004) 163.

K. Fukushima, Phys. Lett. B 591 (2004) 277.

C. Ratti, M.A. Thaler and W. Weise, Phys. Rev. D 73 (2006) 014019.

Experimental Data Analysis:

U.W. Heinz, Proc. *2nd CERN-CLAF School of High Energy Physics*, Mexico City, (2003) 165, `arXiv:hep-ph/0407360`.

B. Abelev *et al.* (STAR Collaboration), Phys. Rev. C 79 (2009) 034909.

S. Weinberg, *Cosmology*, (Oxford, New York, 2008).